Luo *et al. Soft Sci* 2024;4:7
DOI: 10.20517/ss.2023.40

Soft Science

Research Article

Open Access

Check for updates

Printing surface cuprous oxides featured liquid metal for non-enzymatic electrochemical glucose sensor

Yiyao Luo[1,#], Gengcheng Liao[1,#], Zixuan Guo[1], Zongyu Huang[1,3], Long Ren[2,*], Xiang Qi[1,*]

[1]Human Key Laboratory of Micro-Nano Energy Materials and Devices, School of Physics and Optoelectronic, Xiangtan University, Xiangtan 411105, Hunan, China.
[2]State Key Laboratory of Advanced Technology for Materials Synthesis and Processing, International School of Materials Science and Engineering, Wuhan University of Technology, Wuhan 430070, Hubei, China.
[3]Human Key Laboratory of Two-dimensional Materials, Hunan University, Changsha 410082, Hunan, China.
[#]Authors contributed equally.

[*]**Correspondence to:** Prof. Long Ren, State Key Laboratory of Advanced Technology for Materials Synthesis and Processing, International School of Materials Science and Engineering, Wuhan University of Technology, 122 Luoshi Road, Hongshan District, Wuhan 430070, Hubei, China. E-mail: renlong@whut.edu.cn; Prof. Xiang Qi, Human Key Laboratory of Micro-Nano Energy Materials and Devices, School of Physics and Optoelectronic, Xiangtan University, Xinxiang Road, Xianfeng Street, Yuhu District, Xiangtan 411105, Hunan, China. E-mail: xqi@xtu.edu.cn

How to cite this article: Luo Y, Liao G, Guo Z, Huang Z, Ren L, Qi X. Printing surface cuprous oxides featured liquid metal for non-enzymatic electrochemical glucose sensor. *Soft Sci* 2024;4:7. https://dx.doi.org/10.20517/ss.2023.40

Received: 28 Aug 2023 **First Decision:** 27 Sep 2023 **Revised:** 10 Nov 2023 **Accepted:** 7 Dec 2023 **Published:** 15 Jan 2024

Academic Editors: Zhifeng Ren, Chuanfei Guo, Wei Rao **Copy Editor:** Pei-Yun Wang **Production Editor:** Pei-Yun Wang

Abstract

Electrochemical glucose sensors that rely on two-dimensional (2D) oxides have attracted significant attention owing to the strong sensing activity of 2D oxides, but their practical application is hindered by the complexity and high cost of fabrication of electrodes and integrated devices. Herein, a convenient and effective fabrication route that includes printing a Ga-based liquid metal (LM) as a current collection electrode, followed by growing electrochemically active 2D oxides directly on the surface of Ga-based LMs under mild conditions, is developed for non-enzyme-based electrochemical sensors. Specifically, 2D annealed Cu-Oxide (ACO) is successfully grown on a printed Ga electrode through a galvanic replacement reaction, resulting in the formation of a mechanically and electrically well-matched interface between the active sensing materials and the current collection substrate. Benefitting from the high quantity of 2D ACO and good charge transfer at the interface, the as-prepared ACO electrode exhibits attractive glucose sensing performance, with a wide linear range (1 μM-10 mM) of effective detection, low detection limit down to 1 μM, and high sensitivity of 0.87 $\mu A \cdot mM^{-1} \cdot cm^{-2}$. Our study highlights the potential of using LMs in bio-sensing applications and provides a non-enzyme-based electrochemical biosensor platform for effective glucose detection in diets and clinical diagnostic settings.

Keywords: Glucose sensor, liquid metal, cuprous oxide, printing biosensors

INTRODUCTION

Glucose, a vital molecule in the human body, plays a key role in biological cellular processes and clinical diagnoses. Usually, the human body maintains a blood glucose concentration of 4.4-6.6 mM, and excessively high or low blood glucose concentrations can cause various diseases, such as diabetes and hypoglycemia[1]. Thus far, numerous glucose-detection approaches have been studied to fulfill the standard of clinical diagnosis and facilitate daily disease prevention. Among them, electrochemical glucose sensors are considered a promising approach to convert chemical signals into electrical signals owing to their good selectivity, high sensitivity, and compact size[2,3]. Most of the existing electrochemical glucose biosensors utilize an enzyme (normally glucose oxidase enzyme) as the active component that reacts with and detects glucose molecules. However, these enzyme-based electrochemical biosensors are usually limited by enzyme conditions (for example, enzyme activity is directly affected by even slight changes in temperature or pH value)[4,5]. Recently, non-enzyme-based electrochemical glucose biosensors that can easily detect glucose through electrochemical redox reactions have attracted considerable attention. These sensors are more robust and cost-effective compared to enzyme-based electrochemical biosensors[6,7].

In the case of non-enzyme-based glucose sensors, development of electrode materials with good electrochemical activity and effective construction of the electrode system are key challenges from the perspective of improving their glucose detection performance. Notably, two-dimensional (2D) oxides offer attractive advantages in glucose-sensing applications owing to their unique electrochemical capabilities, relatively high surface area, and rapid electron mobility[8,9]. Nevertheless, high energy consumption at the mechanically and electrically mismatched interface between active 2D oxides and the conductive substrate usually degrades the conversion rate of chemical signals to electrical signals, which limits the sensitivity and application range of 2D-oxide-based biosensors[10]. We anticipate that these challenges can be addressed by directly growing 2D oxides on conductive substrates through physical/chemical deposition or wet chemical synthesis[11]. However, the need for extreme fabrication conditions, including high temperatures and excessive chemical treatment, limits the practical application potential of these sensors.

Recently, Ga-based liquid metals (Ga-LM) and related low-melting-point alloys with good fluidity, high conductivity, and good biocompatibility have attracted considerable attention for use in diverse applications, especially flexible electrodes and wearable sensors[12-14]. Particularly, the active and smooth surface of Ga-LM offers an ideal platform for the synthesis of 2D materials under mild growing conditions[15]. For example, various 2D oxides can be grown on the LM surface by inducing a galvanic reaction between the metal atoms on the LM surface and the surrounding ions[16]. Owing to the chemical compatibility of the galvanic reaction and extensibility of post-processing, the 2D oxides synthesized on LM templates are rich and diverse in species. Notably, a 2D oxide layer grown in this manner covers and naturally comes into contact with the highly conductive LM, resulting in the formation of a perfect mechanically and electrically matched interface between the 2D oxides and the conductive substrate[17-20]. This construction scheme can be applied directly to form an integrated electrode decorated with active materials in electrochemical devices. In addition, the deformability of LM imparts high flexibility to the integrated electrode. Therefore, through this strategy, it is believed that a high-performance electrochemical glucose biosensor with good interfacial interaction and flexibility can be achieved based on the combination of 2D oxides and LM.

To validate this concept, cuprous oxide, a representative semiconductive 2D oxide used in glucose sensors owing to its strong catalytic activity, stable structure, and non-toxicity[21,22], is selected as the electrochemically active material herein to construct a non-enzyme-based glucose sensor. The

thermodynamically favorable galvanic reaction between metallic Ga and Cu ions facilitates the direct growth of Cu-based compounds on the Ga-LM surface[23-25]. Accordingly, herein, we propose a simple but highly effective route to synthesize a Ga-LM electrode decorated with a 2D annealed Cu-Oxide (ACO) surface layer for use in non-enzyme-based electrochemical glucose biosensors. By taking advantage of the LM's fluidity[26], a uniform and continuous Ga-LM film is printed on various substrates as the current collector. Then, a high-quality ultrathin 2D ACO layer is grown successfully on the Ga-LM surface by triggering a mild galvanic replacement reaction, which is followed by low-temperature thermal treatment. In this manner, an integrated electrochemical electrode for glucose sensing is realized. This electrode combines the electrochemical sensing capability of ACO, good conductivity of Ga-LM, and good interfacial charge transfer between ACO and Ga-LM. The performance of the proposed glucose-sensing electrode is evaluated using cyclic voltammetry (CV), linear sweep voltammetry, and amperometry, and it exhibits satisfactory sensitivity (0.87 $\mu A \cdot mM^{-1} \cdot cm^{-2}$) and a wide linear detection range (1 $\mu M^{-10} \cdot mM$). Furthermore, the proposed sensor exhibits impressive glucose selectivity, and it can exclude several interfering signals, such as those of sucrose, uric acid (UA), ascorbic acid (AA), and NaCl.

EXPERIMENTAL

Materials

Gallium (bulk, 99.99%) was purchased from Shanghai Aladdin Biochemical Technology Co. Ltd. Copper nitrate hydrate [$Cu(NO_3)_2 \cdot xH_2O$, 99.99%], UA (99%), and AA (99%) were obtained from Shanghai Macklin Biochemical Co. Ltd. Ammonium hydroxide solution (NH_4OH, 25%) was purchased from Sinopharm Chemical Reagent Co. Ltd. Potassium hydroxide pellets (KOH, 85%) and anhydrous sodium sulfate (Na_2SO_4, 99.0%) were procured from Hunan Hui Hong. Ringer's solution and simulated body fluid (SBF) solution (pH 7.4) were purchased from Aladdin. Carbon black (Mw 12.011 g/mol) was purchased from Sigma Aldrich. Flexible polyethylene (PE) and paper substrates were purchased from the market. Sodium chloride (NaCl, AR) and glucose (AR) were purchased from Tianjin Kermel Chemical Reagent Co. Ltd. Indium tin oxide (ITO) conductive glass (surface resistance: 6 Ω/sq, light transmittance: ~84%) was obtained from South China Science and Technology Co. Ltd. All reagents were used directly without further purification.

Sample preparation

The ACO electrode preparation process started with the printing of the Ga-LM electrode. 0.1 g of pure melted Ga was first extruded onto the ITO glass substrate, which resulted in the formation of a well-dispersed liquid Ga layer on the ITO substrate. Then, the liquid Ga layer was subjected to a blade coating process to achieve uniform layer thickness. A simple printing process that combines this coating step with a customized mask can be used to print various conductive patterns as electrodes. The Ga surface is sensitive to oxygen; therefore, a Ga-oxide layer was readily formed after the printing process. In this manner, a GaO_x-Ga electrode was fabricated. The surface of the fabricated GaO_x-Ga electrode was quickly treated with 1 mL of 1 M KOH solution, followed by rinsing with deionized (DI) water. This step was essential for removing the gallium oxide skin formed on the Ga surface. Immediately after this step, the samples were soaked in a solution of 0.01 M $Cu(NO_3)_2$ and NH_4OH (adjusted pH ≈ 11) and allowed to react for 10 min. Thereafter, they were cleaned thrice with DI water and anhydrous ethanol to obtain CuO_x-Ga electrodes. Eventually, these electrodes were dried and annealed for 2 h in a tubular furnace at 200 °C to obtain the final ACO electrode.

Performance measurement

The electrochemical parameters and other response parameters of the fabricated electrodes were measured using a standard electrochemical workstation (CHI660D, Shanghai Chenhua) in the test process. A three-electrode system consisting of the synthesized electrodes was used as the working electrode, a platinum

plate electrode was used as the counter electrode, and an Ag/AgCl electrode was used as the reference electrode. A two-electrode flexible device composed of the synthesized ACO on Ga-LM as the working electrode and carbon black coated on the surface of another batch of isolated Ga-LM as the counter electrode was fabricated. The sensitivity can be calculated as the ratio of the slope to the electrode area, Sensitivity = photocurrent/concentration/area.

Characterizations

The microstructure of ACO and CuO_x-Ga electrodes were observed using scanning electron microscopy (SEM, S-4800) with energy-dispersive X-ray spectroscopy (EDS, Oxford). The Raman spectra and photoluminescence spectra of the ACO electrode were measured at room temperature and excitation wavelength of 532 nm using a WITec-Alpha 300 Raman microscope. The crystal structure and crystallization of the sample were studied using an X-ray diffractometer (XRD-D8 Discover). X-ray photoelectron spectroscopy (XPS) was used in combination with one-chamber electron spectroscopy for chemical analysis (ESCA) to analyze the oxides in these samples.

RESULTS AND DISCUSSION

The ACO electrode was fabricated through a simple printing process of Ga-LM onto the surface of ITO glass, followed by in-situ growth of cuprous oxide on the Ga surface and the final annealing treatment [Figure 1]. Specifically, when the printed Ga-LM electrode came into contact with oxygen, a thin oxide layer was immediately formed on its surface. To remove the surface oxide layer and expose the Ga surface, the electrode was washed with a base[12,27]. Subsequently, galvanic replacement reactions[28] were carried out between $[Cu(OH)_3]^-$ and Ga on the electrode surface, and the final stable ACO layer was formed after annealing.

The morphology of the as-prepared ACO electrode was characterized with SEM, and the resulting mapping images are presented in Figure 2A-C. The SEM characterization results showed a flat surface with several ripples was formed, as depicted in Figure 2A[29]. The inset of Figure 2A shows a high-magnification view of a randomly selected area on the flat ACO surface, and this image clarifies that the flat surface was composed of interconnected nanoparticles. In comparison, as shown in Supplementary Figure 1, while the surface morphology of the CuO_x-Ga electrode is similar, its surface is slightly less smooth, and a few defects exist between the small copper oxide particles. This implies that after annealing treatment, the consistency of the surface layer increased, and interfacial contact between the ACO film and the LM substrate improved. EDS mapping of the ACO electrode shows the relatively homogeneous distribution of elemental Ga, O, Cu, and C throughout the duration of the galvanic reaction and annealing treatment [Figure 2B]. The atomic percentages of Ga, Cu, C, and O were around 85.6%, 1.14%, 6.2%, and 7.06%, respectively, as extracted from the energy spectrum shown in Figure 2C. Owing to the fluidity of the LM, flexible PE, paper, and PE terephthalate (PET) can be used as suitable substrates for printing LM with a uniform distribution [Figure 2D]. After the solution containing $[Cu(OH)_3]^-$ was added and the galvanic reaction was triggered, the color of the electrodes printed on different substrates changed from white to red [Figure 2E]. Accordingly, in addition to preparing ACO electrodes on ITO glass for use in the fabrication of glucose sensor devices, flexible integrated devices can be fabricated using the aforementioned flexible substrates. Figure 2F depicts a flexible integrated glucose sensor device fabricated by printing an LM pattern on a PE substrate. This device is composed of a concentric-ring-shaped two-electrode system, where ACO on Ga-LM is the working electrode, and carbon black on Ga-LM is the counter electrode. The device has good flexibility, and it can be bent to various angles [Figure 2G and H].

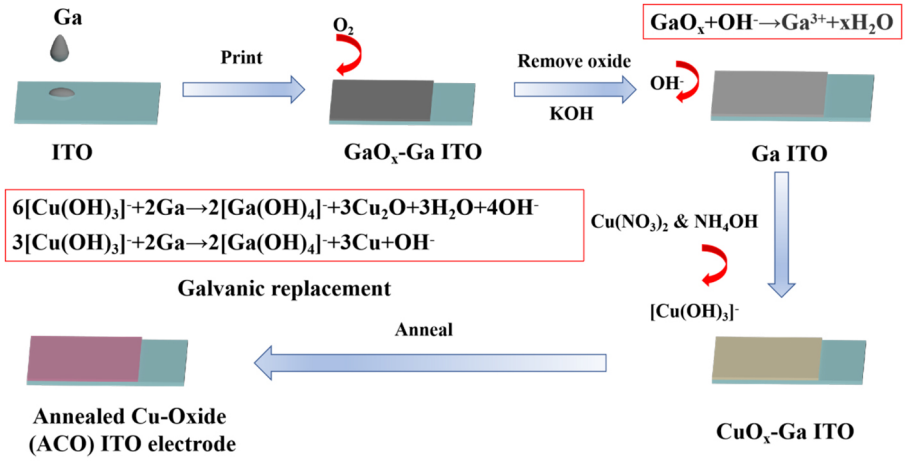

Figure 1. Schematic illustration of ACO electrode synthesis. ACO: Annealed Cu-Oxide; ITO: indium tin oxide.

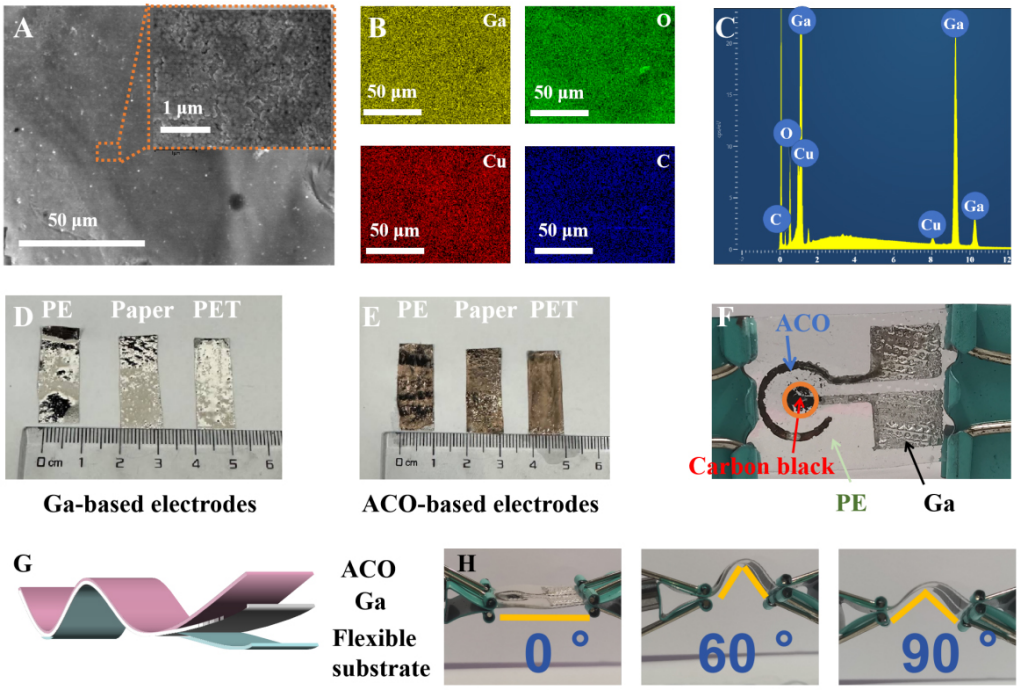

Figure 2. (A) SEM image; (B) corresponding elemental mapping; and (C) EDS spectrum of a typical area on the ACO electrode surface; (D) Images of liquid Ga printed on different substrates, including PE, paper, and PET; (E) Related ACO electrodes printed on PE, paper, and PET substrates; (F) Images of a typical printed two-electrode system with ACO as the working electrode, carbon black as the counter electrode, and PE as the substrate; (G) Schematic representation of the flexible ACO electrode; (H) Photographs of flexible ACO electrodes bent to various angles. ACO: Annealed Cu-Oxide; EDS: energy-dispersive X-ray spectroscopy; PE: polyethylene; PET: PE terephthalate; SEM: scanning electron microscopy.

Before performance evaluation, the surface chemical states of the ACO electrode, along with valence and composition information, were elucidated using XPS. As depicted in Figure 3A, the survey spectra verified the presence of Cu, Ga, and O in the ACO electrode. In addition, the Ga 3d spectrum, presented in Figure 3B, clearly highlighted the three chemical states of Ga: the peaks at 18.1, 19.6, and 20.5 eV were

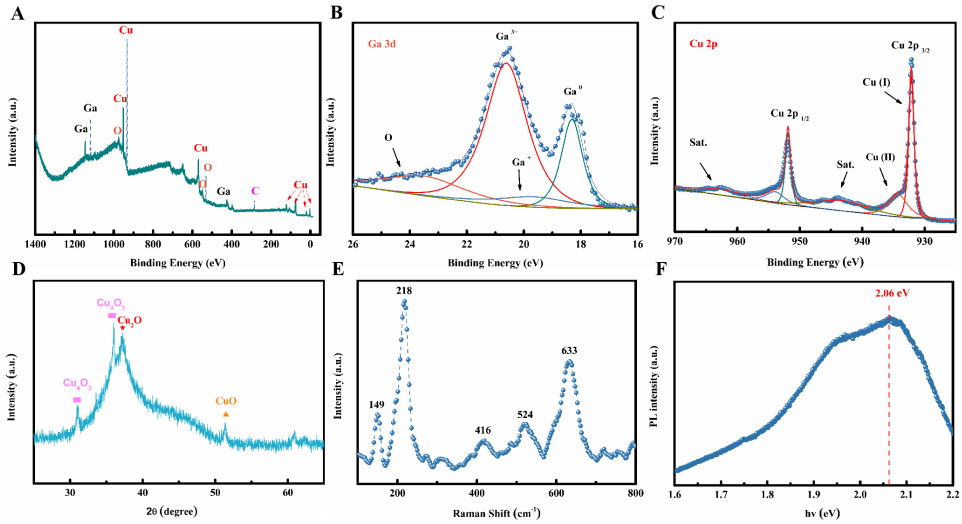

Figure 3. (A) Survey XPS spectra of the ACO electrode; XPS spectra of (B) Ga 3d peaks; (C) Cu 3d peaks; (D) XRD pattern; and (E and F) Raman spectra and photoluminescence spectra of the ACO electrode. ACO: Annealed Cu-Oxide; XPS: X-ray photoelectron spectroscopy; XRD: X-ray diffractometer.

assigned to Ga, Ga_2O, and Ga_2O_3, respectively. The Cu 2p spectra of the ACO electrode are depicted in Figure 3C. The Cu 2p peaks were assigned to two components as follows: those at 932.3 and 951.9 eV were assigned to surface Cu^{2+} species, and those at 934.28 and 954.0 eV were assigned to surface Cu^{+} species[30-32]. The results proved that through Galvanic replacement, a CuO_x film was formed on the electrode surface. The valence state of Cu after annealing treatment was mainly Cu^{+}. Moreover, the elemental composition was analyzed further by using XRD [Figure 3D]. The peaks at 31 and 35.9 were assigned to Cu_4O_3, while the peaks at 37.1 and 51.2 were assigned to Cu_2O and CuO, respectively[33]. Raman spectra of the ACO electrode surface are presented in Figure 3E. The main Raman peaks at 149 cm^{-1} corresponded to the first-order Raman-allowed mode (Γ_{25}) of Cu_2O, while the peaks at 218 and 633 cm^{-1} were assigned to the second-order Raman-allowed mode ($2\Gamma_{12-}$) and infrared-allowed mode [$B^{(2)}_g$] of Cu_2O, respectively[34]. The room-temperature photoluminescence spectra of the ACO electrode excited by a 532 nm laser are depicted in Figure 3F. The emission spectrum exhibits a larger optical peak centered at 2.06 eV, which is close to the optical band gap value, as reported in the literature[35]. These results further confirmed the synthesis of the ACO electrode.

The as-grown ACO on the Ga surface was expected to serve as the active component for electrocatalytic glucose sensing. Thus, the electrocatalytic properties of the ACO electrode were studied using a typical three-electrode electrochemical system [Figure 4]. Figure 4A depicts CV results of the ACO electrode, which were obtained in a 0.5 M Na_2SO_4 solution at various scan rates (20-100 $mV{\cdot}s^{-1}$). The peak current increased as the scanning speed increased. Evidently, the linear variation of the reductive peak current with the square root of the scanning rate, that is, the R^2 of the oxidation peak, was 0.99, while the R^2 of the reduction peak was 0.96. These results indicated that the reaction was diffusion-controlled [Figure 4B]. Figure 4C depicts CV results of the ACO electrode when exposed to different glucose concentrations (0, 2, 4, 6, and 8 mM) at the scan rate of 40 $mV{\cdot}s^{-1}$ in 0.5 M Na_2SO_4. The redox current response of the ACO electrode increased after glucose addition. Figure 4D shows the linear sweep voltammograms (LSV) of the ACO and GaO_x-Ga electrodes when exposed to different glucose concentrations at the scan rate of 10 $mV{\cdot}s^{-1}$. In addition, buffer solutions, which act as electrolytes, were tested herein to verify the reliability of the glucose-sensing tests in body fluid environments. The results of a CV test of the ACO electrode in 0.1 M phosphate buffer solution (PBS) (pH 7.2) indicated that the reaction was more effective at negative

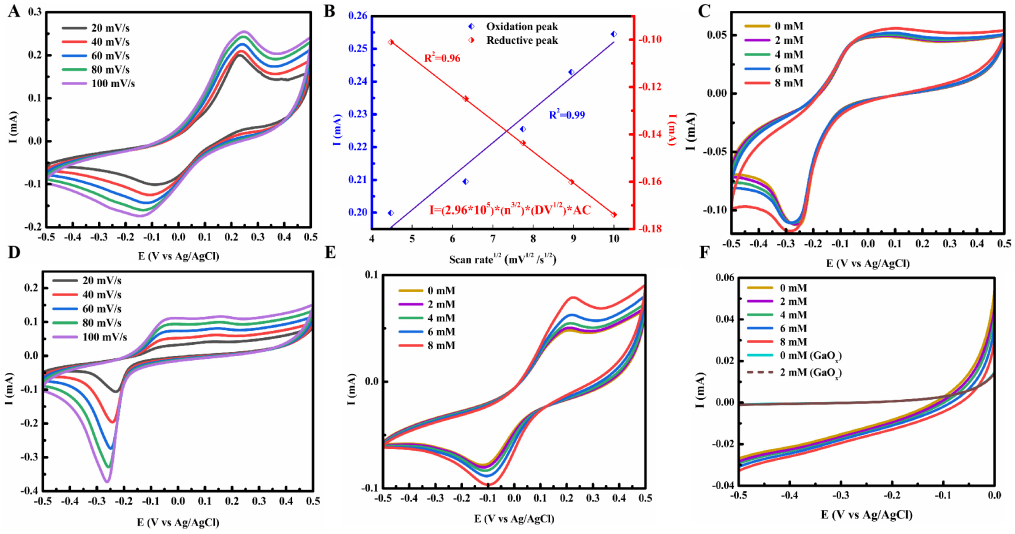

Figure 4. (A) CV curves of the ACO electrode in 0.5 M Na_2SO_4 at different scan rates; (B) Plots of peak current density *vs.* scan rate$^{1/2}$; (C) CV curves of the ACO electrode exposed to different glucose concentrations (0, 2, 4, 6, and 8 mM) in 0.5 M Na_2SO_4; (D) LSV results of ACO and GaO_x-Ga electrodes exposed to different glucose concentrations in 0.5 M Na_2SO_4 at negative bias voltage; (E) CV curves of the ACO electrode in 0.1 M PBS (pH 7.2) at different scan rates; (F) CV curves of the ACO electrode exposed to different glucose concentrations (0, 2, 4, 6, and 8 mM) in 0.1 M PBS (pH 7.2). ACO: Annealed Cu-Oxide; CV: cyclic voltammetry; LSV: linear sweep voltammograms; PBS: phosphate buffer solution.

voltages [Figure 4E and F]. Supplementary Figure 2 shows the results of similar tests of the ACO electrode in Ringer's Solution containing 0.1 mol/L NaCl and SBF solution containing 0.1 mol/L NaCl, and both sets of results confirmed that the as-prepared ACO electrode exhibited great glucose-sensing responses in these buffer solutions. These results indicate that the ACO electrode exhibited a certain electrocatalytic efficiency in the glucose oxidation process, while the Ga-LM electrodes exhibited almost zero activity in the same process.

Normally, the applied potential strongly influences the amperometric response of an electrochemical sensing system to glucose. Figure 5A illustrates the amperometric response of the proposed system to 1 mM glucose in 0.5 M Na_2SO_4 at various applied potentials. The current response increased as the applied potential was increased from 0 to -0.5 V. Nevertheless, to achieve high selectivity and avoid electrochemical corrosion of the LM at higher potentials, -0.4 V was selected as the ideal detection potential for further amperometric measurements. A chronoamperometry test was performed to evaluate the effective linear range and sensitivity of the ACO electrode, wherein different glucose concentrations were added to 50 mL of 0.5 M Na_2SO_4 at intervals of 25 s under an applied potential of -0.4 V. The amperometric response results are presented in Figure 5B. Upon glucose addition, the current increased gradually, indicating that the ACO electrode exhibited effective electrocatalytic ability for glucose oxidation. Moreover, a linear relationship was observed between the current response and added glucose concentration across various concentration ranges. The corresponding linear regression equations are as follows [Figure 5C]:

$$I\ (\mu A) = -21.77\ C\ (mM) - 22.21\ (1\ \mu M - 100\ \mu M)\ R^2 = 0.87 \quad (1)$$

$$I\ (\mu A) = -2.42\ C\ (mM) - 23.72\ (100\ \mu M - 1.6\ mM)\ R^2 = 0.98 \quad (2)$$

$$I\ (\mu A) = -1.07\ C\ (mM) - 25.85\ (1.6\ mM - 10\ mM)\ R^2 = 0.99 \quad (3)$$

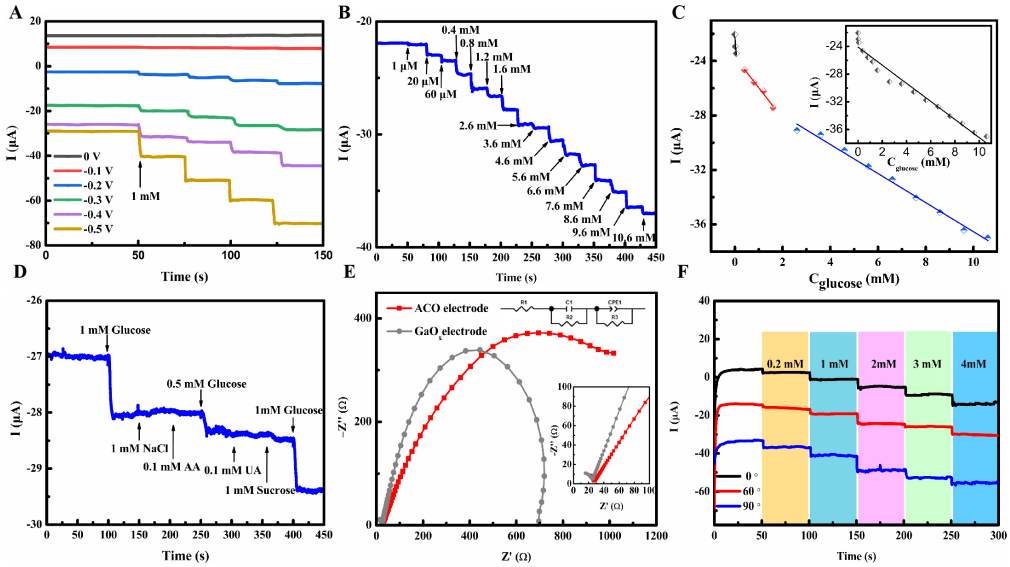

Figure 5. (A) Effect of applied potential on amperometric response of the sensor to 1 mM glucose in 0.5 M Na_2SO_4; (B) Amperometric response curves of the ACO electrode for different glucose concentrations in 0.5 M Na_2SO_4 under an applied potential of -0.4 V (*vs.* Ag/AgCl); (C) Calibration plot of current response *vs.* different glucose concentrations with fitted lines of 1-100 μM, 100 μM-1.6 mM, 1.6-10 mM (the inset image corresponds to the concentration ranges of 1 μm-10 mM); (D) Amperometric responses of the ACO electrode to successive dropwise additions of glucose and interfering species (AA, UA, Sucrose, and NaCl) at -0.4 V (*vs.* Ag/AgCl); (E) EIS results of ACO and GaO_x-Ga electrodes in 0.5 M Na_2SO_4. The inset shows the equivalent impedance circuit; (F) Amperometric response curves of flexible sensors with ACO electrode in bent states of 0°, 60°, and 90° to glucose in 0.5 M NaCl-PVA electrolyte under the applied potential of -0.7 V. AA: Ascorbic acid; ACO: annealed Cu-Oxide; EIS: electrochemical impedance spectroscopy; UA: uric acid.

$$I\ (\mu A) = -1.31\ C\ (mM) - 24.09\ (1\ \mu M - 10\ mM)\ R^2 = 0.96 \quad (4)$$

Furthermore, the sensing electrode exhibited an appropriate sensitivity of 0.87 $\mu A \cdot mM^{-1} \cdot cm^{-2}$ with a comparatively low detection limit of 1 μM. The key issue affecting non-enzyme-based electrochemical sensors is an accurate distinction between the target analytes and the multitude of interfering species. For verifying the anti-interference ability of the ACO electrode, several organic and inorganic substances that are commonly found in the human body, such as NaCl (1 mM), AA (0.1 mM), UA (0.1 mM), and sucrose (1 mM), were successively added to 0.5 M Na_2SO_4 at -0.4 V to explore the selectivity of the glucose sensor fabricated herein. As illustrated in Figure 5D, a significant response to glucose was observed, while the responses to the organic interferences AA and UA were negligible. Furthermore, the sensor exhibited minor responses to 1 mM Cl^- and sucrose, but these responses were weaker than its response to glucose. These research data proved the good selectivity of the ACO electrode. Meanwhile, Figure 5E depicts the electrochemical impedance spectroscopy (EIS) Nyquist plots of the ACO and GaO_x-Ga electrodes from 1 MHz to 0.1 Hz. The two electrodes exhibited similar contact resistance, but their semicircle radians were different. The inset image shows the equivalent impedance circuit. Therefore, the charge transfer resistance of the ACO electrode was higher than that of the GaO_x-Ga electrode, which indicated that the ACO had higher electro-activity. In addition to evaluating the glucose-sensing performance of the typical three-electrode system, the fabricated flexible two-electrode device [Figure 2F-H] was applied directly as a glucose sensor. Figure 5F shows the amperometric response curves of the flexible device to glucose in 0.5 M Na_2SO_4 under an applied potential of -0.7 V in bent states of 0°, 60°, and 90°. The fabricated flexible device with the proposed ACO electrode exhibited good glucose response at various bending angles, which indicated that the interfacial contact between the LM and surface copper oxide was good. For comparison, the determination performance of the ACO electrode fabricated in this work was compared to those of non-enzymatic glucose sensors based on other reported materials, as summarized in Table 1. Compared to the

Table 1. Comparison of behavior of flexible sensors based on the ACO electrode with those of non-enzymatic glucose sensors based on other reported materials

Materials	Electrode fabrication	Limit of detection (μM)	Sensitivity $\mu A \cdot mM^{-1} \cdot cm^{-2}$	Applied potential (V)	Flexibility	Ref.
Si-CuO core-shell nanowire	MPI method; E evaporator	740	2,324.09	1.0 (*vs.* Ag/AgCl)	×	[40]
Cu_2O/TiO_2	A JDF-05 benchtop machine at an applied voltage of 21 kV and a propulsion rate of 1.0 mL/h; 600 °C	14.4	1.0366	0.1 (*vs.* Hg/HgO)	×	[41]
CuO	450 °C at atmospheric pressure; NH_3; 650 °C	59	263	0.54 (n/A)	×	[42]
Cu/Cu_2O	700 °C	0.31	621.12	0.4 (n/A)	×	[43]
$Au@CuO/V_2CT_x$	HF aqueous, argon, vigorous stirring, low temperature	5	1.124×10^6	0.45 (*vs.* SCE)	×	[44]
MXene/NiCo-LDH	HF, vacuum, centrifugation, high temperature	0.53	67.75	0.45 (*vs.* SCE)	×	[45]
$Ti_3C_2T_x$-Cu_2O	Centrifugation, vacuum, HF, high temperature	10	11.061	0.6 (*vs.* Ag/AgCl)	×	[46]
Pt/MXene/CH/Pt	HCl, high temperature, lithography	29.15	3.43	0.2 (*vs.* Ag/AgCl)	√	[47]
ACO	Room temperature	1	0.87	-0.4 (*vs.* Ag/AgCl)	√	This work

ACO: Annealed Cu-Oxide; CH: conductive hydrogel; HF: hydrofluoric acid ; LDH: layered double hydroxide ; MPI: micro-propulsive injection; SCE: saturated calomel electrode.

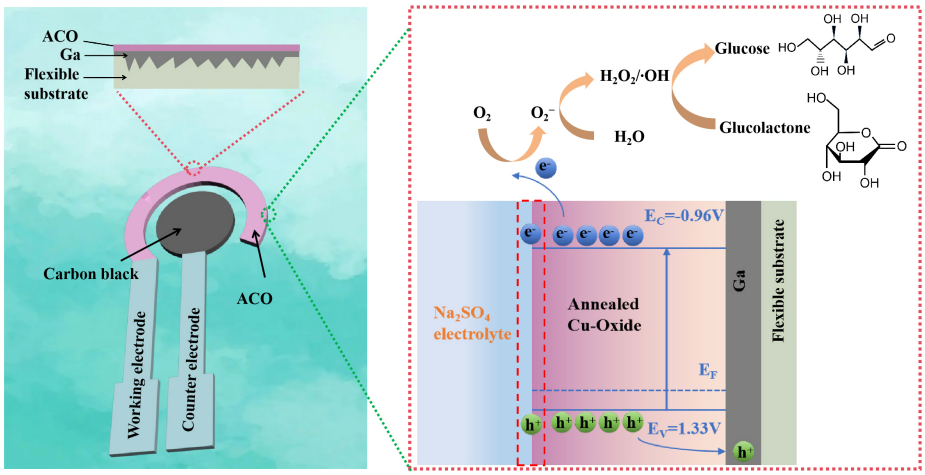

Figure 6. Schematic of electrochemical oxidation of glucose on the surface of the ACO electrode. ACO: Annealed Cu-Oxide.

sensors based on the other materials, the sensor based on the proposed ACO electrode exhibited superior flexibility, higher sensitivity, and lower limit of detection.

The electrochemical oxidation mechanism of glucose at the ACO electrode is depicted in Figure 6. Owing to the strong O_2 adsorption capacity of cuprous oxide, under the externally applied negative potential, cuprous oxide facilitated the transformation of O_2 into O_2^- [Equation (5)][36]. O_2^- further reacted with H_2O and electrons to produce H_2O_2 and hydroxyl radicals (·OH) [Equations (6) and (7)][37,38]. These strongly oxidizing ·OH radicals initiated the auto-oxidation of glucose to produce glucolactone [Equation (8)][39].

$$Cu_2O + O_2 + e^- \rightarrow Cu_2O + O_2^- \quad (5)$$

$$O_2^- + H_2O \rightarrow H_2O_2 + \cdot OH \quad (6)$$

$$O_2^- + H_2O_2 \rightarrow H_2O + \cdot OH + O_2 \quad (7)$$

$$\cdot OH + glucose \rightarrow glucolactone \quad (8)$$

Then, the electrons produced by the electrochemical oxidation of glucose were transferred to the external circuit through the working electrode, which generated a current signal. As discussed above, cuprous oxide enhanced the electrocatalytic activity of the ACO electrode by producing O_2^- and ·OH, leading to glucose oxidation at negative potentials.

CONCLUSIONS

In sum, we proposed a novel approach to prepare a highly sensitive, non-enzyme-based electrode with good selectivity for electrochemical glucose sensing by directly printing Ga-LM on an ITO or PE substrate and realizing galvanic replacement in situ growth of cuprous oxide on Ga-LM. The characterizations and electrochemical measurements of the as-prepared electrode revealed the successful fabrication of cuprous oxide, and the proposed electrode can potentially be applied in enzyme-free electrochemical sensing schemes. Owing to mechanical and electrical synergy of the ACO, the ACO electrode exhibited high sensitivity in the glucose detection over a wide glucose concentration range of 1 μM-10 mM. In addition, the sensor exhibited a low detection limit and good selectivity for glucose. The glucose sensor fabricated herein has great potential for use in the detection of human serum glucose, dietary glucose, and clinical diagnoses.

DECLARATIONS

Authors' contributions

Made substantial contributions to the conception and design of the study: Ren L, Liao G
Performed data analysis and interpretation and wrote the manuscript: Luo Y, Liao G, Guo Z
Provided administrative, technical, and material support: Qi X, Ren L, Huang Z

Availability of data and materials

Not applicable.

Financial support and sponsorship

This work was supported by Grants from the National Natural Science Foundation of China (No. 52201164, No. 12274359), Fundamental Research Funds for the Central Universities (WUT: 2022IVA187), Natural Science Fund for Distinguished Young Scholars of Hunan Province (No. 2023JJ10037), Scientific Research Fund of Hunan Provincial Education Department (No. 21B0128), and Postgraduate Scientific Research Innovation Project of Hunan Province (No. CX20230548).

Conflicts of interest

All authors declared that there are no conflicts of interest.

Ethical approval and consent to participate

Not applicable.

Consent for publication

Not applicable.

REFERENCES

1. Taylor PJ, Thompson CH, Brinkworth GD. Effectiveness and acceptability of continuous glucose monitoring for type 2 diabetes management: a narrative review. *J Diabetes Investig* 2018;9:713-25. DOI
2. Wang M, Song X, Song B, et al. Precisely quantified catalyst based on in situ growth of Cu_2O nanoparticles on a graphene 3D network for highly sensitive glucose sensor. *Sensor Actuat B Chem* 2017;250:333-41. DOI
3. Zhang C, Zhang Z, Yang Q, Chen W. Graphene-based electrochemical glucose sensors: fabrication and sensing properties. *Electroanalysis* 2018;30:2504-24. DOI
4. Vashist SK. Non-invasive glucose monitoring technology in diabetes management: a review. *Anal Chim Acta* 2012;750:16-27. DOI
5. Lee WC, Kim KB, Gurudatt NG, et al. Comparison of enzymatic and non-enzymatic glucose sensors based on hierarchical Au-Ni alloy with conductive polymer. *Biosens Bioelectron* 2019;130:48-54. DOI
6. Niu X, Li X, Pan J, He Y, Qiu F, Yan Y. Recent advances in non-enzymatic electrochemical glucose sensors based on non-precious transition metal materials: opportunities and challenges. *RSC Adv* 2016;6:84893-905. DOI
7. Xiao X, Peng S, Wang C, et al. Metal/metal oxide@carbon composites derived from bimetallic Cu/Ni-based MOF and their electrocatalytic performance for glucose sensing. *J Electroanal Chem* 2019;841:94-100. DOI
8. Zhao Y, Li W, Pan L, et al. ZnO-nanorods/graphene heterostructure: a direct electron transfer glucose biosensor. *Sci Rep* 2016;6:32327. DOI
9. Huang W, Ding S, Chen Y, et al. 3D NiO hollow sphere/reduced graphene oxide composite for high-performance glucose biosensor. *Sci Rep* 2017;7:5220. DOI
10. Mei LP, Song P, Feng JJ, et al. Nonenzymatic amperometric sensing of glucose using a glassy carbon electrode modified with a nanocomposite consisting of reduced graphene oxide decorated with Cu_2O nanoclusters. *Microchim Acta* 2015;182:1701-8. DOI
11. Sheng X, Xu T, Feng X. Rational design of photoelectrodes with rapid charge transport for photoelectrochemical applications. *Adv Mater* 2019;31:1805132. DOI
12. Lin Y, Genzer J, Dickey MD. Attributes, fabrication, and applications of gallium-based liquid metal particles. *Adv Sci* 2020;7:2000192. DOI
13. Yan J, Lu Y, Chen G, Yang M, Gu Z. Advances in liquid metals for biomedical applications. *Chem Soc Rev* 2018;47:2518-33. DOI
14. Zhang BW, Ren L, Wang YX, Xu X, Du Y, Dou SX. Gallium-based liquid metals for lithium-ion batteries. *Interdiscip Mater* 2022;1:354-72. DOI
15. Hoshyargar F, Crawford J, O'Mullane AP. Galvanic replacement of the liquid metal galinstan. *J Am Chem Soc* 2017;139:1464-71. DOI
16. Ren L, Cheng N, Man X, et al. General programmable growth of hybrid core-shell nanostructures with liquid metal nanodroplets. *Adv Mater* 2021;33:2008024. DOI
17. Daeneke T, Khoshmanesh K, Mahmood N, et al. Liquid metals: fundamentals and applications in chemistry. *Chem Soc Rev* 2018;47:4073-111. DOI
18. Syed N, Zavabeti A, Mohiuddin M, et al. Sonication-assisted synthesis of gallium oxide suspensions featuring trap state absorption: test of photochemistry. *Adv Funct Mater* 2017;27:1702295. DOI
19. Zhao H, Wang C, Liu G, et al. Efficient and stable hydrogen evolution based on earth-abundant SnSe nanocrystals. *Appl Catal B Environ* 2020;264:118526. DOI
20. Alsaif MMYA, Haque F, Alkathiri T, et al. 3D visible-light-driven plasmonic oxide frameworks deviated from liquid metal nanodroplets. *Adv Funct Mater* 2021;31:2106397. DOI
21. Lu W, Sun Y, Dai H, et al. Direct growth of pod-like Cu_2O nanowire arrays on copper foam: highly sensitive and efficient nonenzymatic glucose and H_2O_2 biosensor. *Sensor Actuat B Chem* 2016;231:860-6. DOI
22. He J, Jiang Y, Peng J, Li C, Yan B, Wang X. Fast synthesis of hierarchical cuprous oxide for nonenzymatic glucose biosensors with enhanced sensitivity. *J Mater Sci* 2016;51:9696-704. DOI
23. Amirzadeh Z, Javadpour S, Shariat MH, Knibbe R. Non-enzymatic glucose sensor based on copper oxide and multi-wall carbon nanotubes using PEDOT:PSS matrix. *Synth Met* 2018;245:160-6. DOI
24. Khedekar VV, Bhanage BM. Simple electrochemical synthesis of cuprous oxide nanoparticles and their application as a non-enzymatic glucose sensor. *J Electrochem Soc* 2016;163:B248. DOI
25. Laidoudi S, Khelladi MR, Lamiri L, et al. Non-enzymatic glucose detection based on cuprous oxide thin film synthesized via electrochemical deposition. *Appl Phys A* 2021;127:160. DOI
26. Neumann TV, Dickey MD. Liquid metal direct write and 3D printing: a review. *Adv Mater Technol* 2020;5:2000070. DOI
27. Eaker CB, Dickey MD. Liquid metal actuation by electrical control of interfacial tension. *Appl Phys Rev* 2016;3:031103. DOI

28. Ropp RC. Encyclopedia of the alkaline earth compounds. 1st ed. Elsevier Pul. Co; 2013. DOI
29. Wang Y, Li Y, Zhang J, Zhuang J, Ren L, Du Y. Native surface oxides featured liquid metals for printable self-powered photoelectrochemical device. *Front Chem* 2019;7:356. DOI
30. Ren T, Yu Z, Yu H, et al. Interfacial polarization in metal-organic framework reconstructed Cu/Pd/CuO_x multi-phase heterostructures for electrocatalytic nitrate reduction to ammonia. *Appl Catal B Environ* 2022;318:121805. DOI
31. Lyu Z, Zhu S, Xie M, et al. Controlling the surface oxidation of Cu nanowires improves their catalytic selectivity and stability toward C_{2+} products in CO_2 reduction. *Angew Chem Int Ed Engl* 2021;60:1909-15. DOI
32. Wang Y, Zhou W, Jia R, Yu Y, Zhang B. Unveiling the activity origin of a copper-based electrocatalyst for selective nitrate reduction to ammonia. *Angew Chem Int Ed Engl* 2020;59:5350-4. DOI
33. Lv J, Wu S, Tian Z, Ye Y, Liu J, Liang C. Construction of PdO-Pd interfaces assisted by laser irradiation for enhanced electrocatalytic N_2 reduction reaction. *J Mater Chem A* 2019;7:12627-34. DOI
34. Powell D, Compaan A, Macdonald JR, Forman RA. Raman-scattering study of ion-implantation-produced damage in Cu_2O. *Phys Rev B* 1975;12:20. DOI
35. Balık M, Bulut V, Erdogan IY. Optical, structural and phase transition properties of Cu_2O, CuO and Cu_2O/CuO: their photoelectrochemical sensor applications. *Int J Hydrogen Energ* 2019;44:18744-55. DOI
36. Li Q, Xu P, Zhang B, et al. Structure-dependent electrocatalytic properties of Cu_2O nanocrystals for oxygen reduction reaction. *J Phys Chem C* 2013;117:13872-8. DOI
37. Lee JH, Shoeman DW, Kim SS, Csallany AS. The effect of superoxide anion in the production of seven major cholesterol oxidation products in aptoric and protic conditions. *Int J Food Sci Nutr* 1997;48:151-9. DOI
38. Khaliq N, Rasheed MA, Cha G, et al. Development of non-enzymatic cholesterol bio-sensor based on TiO_2 nanotubes decorated with Cu_2O nanoparticles. *Sensor Actuat B Chem* 2020;302:127200. DOI
39. Fang Q, Qin Y, Wang H, et al. Ultra-low content bismuth-anchored gold aerogels with plasmon property for enhanced nonenzymatic electrochemical glucose sensing. *Anal Chem* 2022;94:11030-7. DOI
40. Zhang R, Ke S, Lu W, et al. Constructing a Si-CuO core-shell nanowire heterojunction photoanode for enzyme-free and highly-sensitive glucose sensing. *Appl Surf Sci* 2023;632:157593. DOI
41. Gao T, Li TT, Liao X, Lin JH, Shiu BC, Lou CW. Construction of Cu_2O/TiO_2 heterojunction photoelectrodes for photoelectrochemical determination of glucose. *J Mater Res Technol* 2022;21:798-809. DOI
42. Cory NJ, Visser E, Chamier J, Sackey J, Cummings F, Chowdhury M. Electrodeposited CuO thin film for wide linear range photoelectrochemical glucose sensing. *Appl Surf Sci* 2022;576:151822. DOI
43. Zhuang X, Han C, Zhang J, Sang Z, Meng W. Cu/Cu_2O heterojunctions in carbon framework for highly sensitive detection of glucose. *J Electroanal Chem* 2021;882:115040. DOI
44. Cui F, Sun H, Yang X, et al. Laser-induced graphene (LIG)-based Au@CuO/V_2CT_x MXene non-enzymatic electrochemical sensors for the urine glucose test. *Chem Eng J* 2023;457:141303. DOI
45. Li M, Fang L, Zhou H, et al. Three-dimensional porous MXene/NiCo-LDH composite for high performance non-enzymatic glucose sensor. *Appl Surf Sci* 2019;495:143554. DOI
46. Gopal TS, Jeong SK, Alrebdi TA, et al. MXene-based composite electrodes for efficient electrochemical sensing of glucose by non-enzymatic method. *Mater Today Chem* 2022;24:100891. DOI
47. Li QF, Chen X, Wang H, Liu M, Peng HL. Pt/MXene-based flexible wearable non-enzymatic electrochemical sensor for continuous glucose detection in sweat. *ACS Appl Mater Interfaces* 2023;15:13290-8. DOI